

Article

Impedimetric Biosensor Coated with Zinc Oxide Nanorods Synthesized by a Modification of the Hydrothermal Method for Antibody Detection

Nikita Sitkov ^{1,2,*} , Andrey Ryabko ^{3,*}, Alexey Kolobov ^{2,4}, Aleksandr Maximov ¹, Vyacheslav Moshnikov ¹ , Stanislav Pshenichnyuk ⁵ , Alexei Komolov ⁶ , Andrey Aleshin ³  and Tatiana Zimina ^{1,2}

- ¹ Department of Micro and Nanoelectronics, Saint Petersburg Electrotechnical University “LETI”, Saint Petersburg 197022, Russia; aimaximov@mail.ru (A.M.); vamoshnikov@mail.ru (V.M.); tmzimina@gmail.com (T.Z.)
- ² Centre for Digital Telecommunication Technologies, Saint Petersburg Electrotechnical University “LETI”, Saint Petersburg 197022, Russia; alexey.kolobov.spb@gmail.com
- ³ Laboratory of Nonequilibrium Processes in Semiconductors, Ioffe Institute, 26 Politekhnicheskaya, Saint Petersburg 194021, Russia; aleshin.transport@mail.ioffe.ru
- ⁴ Laboratory of Peptide Chemistry, Institute of Human Hygiene, Occupational Pathology and Ecology, Saint-Petersburg 188663, Russia
- ⁵ Laboratory of Physics of Atomic Collisions, Institute of Molecule and Crystal Physics, Ufa Federal Research Centre, Russian Academy of Sciences, Prospekt Oktyabrya 151, Ufa 450075, Russia; sapsh@anrb.ru
- ⁶ Solid State Electronics Department, Saint Petersburg State University, Saint Petersburg 199034, Russia; a.komolov@spbu.ru
- * Correspondence: sitkov93@yandex.ru (N.S.); a.a.ryabko93@yandex.ru (A.R.)



Citation: Sitkov, N.; Ryabko, A.; Kolobov, A.; Maximov, A.; Moshnikov, V.; Pshenichnyuk, S.; Komolov, A.; Aleshin, A.; Zimina, T. Impedimetric Biosensor Coated with Zinc Oxide Nanorods Synthesized by a Modification of the Hydrothermal Method for Antibody Detection. *Chemosensors* **2023**, *11*, 66. <https://doi.org/10.3390/chemosensors11010066>

Academic Editor: Xiaolong Yang

Received: 10 December 2022

Revised: 28 December 2022

Accepted: 11 January 2023

Published: 13 January 2023



Copyright: © 2023 by the authors. Licensee MDPI, Basel, Switzerland. This article is an open access article distributed under the terms and conditions of the Creative Commons Attribution (CC BY) license (<https://creativecommons.org/licenses/by/4.0/>).

Abstract: Impedimetric biosensors are used for detecting a wide range of analytes. The detection principle is a perspective for the development of new types of analytical devices for biomolecular diagnosis of diseases. Of particular interest are biosensors with very high sensitivities, capable of detecting trace amounts of biomarkers or drugs in biological fluids. Impedimetric biosensors possess a potential for increased sensitivity, since their electrodes can be modified with nanostructured materials, in particular zinc oxide. In this work, a miniature biosensor with an array of zinc oxide nanorods synthesized by the hydrothermal method has been created. Protein A was immobilized on the resulting structure, which was previously tested for binding to omalizumab by capillary electrophoresis. Using impedance spectroscopy, it was possible to detect the binding of omalizumab at concentrations down to 5 pg/mL. The resulting structures are suitable for creating reusable biosensor systems, since ZnO-coated electrodes are easily cleaned by photocatalytic decomposition of the bound molecules. The biosensor is promising for use in Point-of-Care systems designed for fast, multimodal detection of molecular markers of a wide range of diseases.

Keywords: impedimetric biosensor; zinc oxide; express detection; nanorods; antibodies; label-free detection; hydrothermal synthesis

1. Introduction

The use of micro- and nano-technologies in biology and medicine makes it possible to develop new miniature devices for expressing the control of biological parameters, including multiparametric molecular biomarker monitoring. The main areas of development are biosensors [1,2], lab-on-a-chip (LoC) [3,4] devices and, based on these, portable diagnostic devices in the Point-of-Care Testing (PoCT) [5] class. A biosensor is an analytical device that converts a chemical or physical stimulus derived by an interaction with a biological component into a measurable signal. The following main components form the structure of a biosensor: a biorecognition element (antibody, protein, aptamer, nucleic

acid, microorganism, etc.), which has a specific complementarity to the analyzed object; a transducer (optical, electrochemical, magnetic, etc.), which converts the biointeraction into a recorded and measured signal; and a data processing and analysis system that visualizes and converts experimental data into a form convenient for the operator. Such devices should provide high sensitivity and speed of analysis, use a small sample volume and be of low cost [6].

Antibodies are one of the most popular objects for fast diagnostic devices due to their high specificity and high binding strength to the target. Antibodies are either monoclonal or polyclonal. Monoclonal antibodies are produced by B cells that are clones of the same parent cell and are monovalent when they recognize the same antigen epitope [7]. This type of antibody is produced *ex vivo* in tissue culture. To create polyclonal antibodies, an antigen is injected into an animal that has an immune response, after which they are collected directly from the serum and purified. They can be used as markers for diagnosing chronic [8], neurodegenerative [9,10], oncological [11] and infectious [12] diseases, etc. Traditional methods for the detection of protein biomarkers, such as immunoassays (ELISA, immunochemiluminescent assays), despite their high sensitivity and selectivity, are expensive, time-consuming and multi-stage procedures performed in specialized diagnostic laboratories [13]. Therefore, there is a need to create highly sensitive, fast diagnostic biosensor systems capable of detecting the level of various antibodies at extremely low concentrations.

Optical and electrochemical detection systems are widely used to create miniature devices for protein detection [14,15]. Optical detection methods, which are considered very sensitive and specific, are based on a change in the phase, amplitude, polarization or frequency of incoming light in response to biorecognition processes. Often, these methods use specialized labels, which make it possible to increase sensitivity, but complicate and increase the cost of the manufacturing technology. In addition, the instrumental implementation of individual methods can be large and expensive and require specially trained personnel to conduct tests.

Electrochemical biosensors are one of the most widespread classes of biosensor devices, which use electrodes with recognition elements immobilized on their surface capable of selectively binding to target molecules. Detection of the binding of the target to the recognizer on the electrode is carried out by registering changes in current and/or voltage. According to the measurement principle, electrochemical biosensors are divided into potentiometric, amperometric and impedimetric detection systems that convert a chemical reaction parameter into a measurable electrical signal. Due to low operating voltages, fabrication costs and ease of miniaturization, electrochemical biosensors have great prospects for various biomedical applications, especially for fast, multimodal biosensor systems.

Biosensor systems based on impedance detection are currently one of the most popular solutions for the detection of binding of antibody biomarkers. Unlike other electrochemical methods, impedimetry works on low-amplitude electrical signal disturbances; therefore, this method is considered non-destructive [16]. Since the signal measurement principle of impedance spectroscopy is based on modifications of the electrode surface, it is largely sensitive to the organization of the near-electrode monolayer and can be used for measurements at low concentrations or in studying enzymatic processes [17]. The low cost, speed and convenience of analysis, the possibility of eliminating the influence of third-party substances on the test sample, as well as the ease of miniaturization of such sensors make them promising for integration into LoC. The work [18] is an example of an impedimetric biosensor for the qualitative detection of antibodies of COVID-19 in serum by using gold electrodes deposited on a SiO₂ substrate modified with the SARS-Cov-2 spike protein. The resulting device made it possible to register the specific interaction between the spike protein and antibodies in the studied samples. Soma et al. [19] reported the development of an impedimetric biosensor for the detection of the norovirus with a detection limit of 60 µg/l, where a gold electrode was modified with polyaniline and streptococcus to improve the electron transfer process and the conjugation of a biotinylated monoclonal

antibody, which improves the electrochemical response and provides enhanced active centers for targeted analytes.

Modern biosensors are an example of the convergence of various scientific and technical areas. The use of a variety of nanomaterials (magnetic nanoparticles, nanorods, carbon nanotubes, graphene, quantum dots, etc.) is one of the main means of increasing the sensitivity and selectivity of biosensors [20–22]. Zinc oxide nanostructures are promising in electrochemical biosensors, as they serve in immobilizing a bioselective element and distributing it over the entire electrode area [23–30]. In [23], an example of using zinc oxide nanorods as a layer on the surface of a biosensor is presented, which makes it possible to detect the HRP antigen and nonspecific antigen in the buffer. This result was confirmed by capacitive measurements. The authors found the maximum response for their structure was in the range of 5–6 kHz, which is promising for the creation of a single-frequency measuring system for the analysis of multiple samples. Shanmugam et al. [25] used zinc oxide nanostructures to create a biosensor with multiplex detection of a panel of cardio-biomarkers. The nanostructures were hydrothermally grown, functionalized with specific antibodies and thus prepared to detect cardiac Troponin I and Troponin T with a detection limit of 1 pg/mL.

Zinc oxide is a direct-gap semiconductor with a band gap $E_g \approx 3.3$ eV, n-type conductivity, piezoelectric properties and a high electron mobility [31]. However, interest in zinc oxide is due not only to its electrophysical properties, but also due to the possibility of synthesizing ZnO in the form of nanorods using the hydrothermal method at low (<100 °C) temperatures. This eliminates the use of autoclaves and makes the synthesis of ZnO nanorods scalable and inexpensive, which is extremely important for the creation of disposable biochips. Low-temperature hydrothermal synthesis may be preferable in comparison to physical methods of synthesis, not only due to the possibility of scaling; an advantage of the method is the ability to introduce impurities (dopants) into the synthesis process. The introduction of salts of other metals into the growth solution can modify the surface of nanoparticles with new adsorption centers to improve further binding.

ZnO nanoparticles in the form of nanorods are efficient when treating the substrate surface, since the surface area for immobilization of the bioselective element is considerably higher. This feature makes ZnO nanorods attractive for use in gas sensors [32,33]. ZnO nanorods have also been successfully used as a photocatalyst, where ZnO with high concentrations of OH groups on its surface demonstrated a high photocatalytic activity [34,35]. We assume that such a surface should facilitate immobilization. It should be noted that the possibility of photocatalytic decomposition of molecular units conjugated on the surface of ZnO nanorods can probably ensure the reusability of electrodes coated with ZnO nanorods. The process of biorecognition will be followed by the illumination of the electrodes in the ultraviolet (<380 nm) region and photocatalytic decomposition on the surface of ZnO. After the photocatalysis, the stages of purification and immobilization can be repeated. Therefore, we assume that the use of photocatalytically active materials is especially promising for implementation of reusable sensor chips.

The synthesis methods of ZnO nanorods can be divided into two main approaches: physical gas-phase synthesis methods (including the vapor–liquid–solid method [36], pulsed laser deposition [37], chemical vapor deposition [38,39], molecular beam epitaxy [40] and others) and chemical methods (including such methods as the electrochemical method [41], electrospinning process [42] and others). Nevertheless, the most flexible chemical method is hydrothermal [43,44]. This method, convenient for laboratory application as well as for scaling up, has generated additional interest in the wide study and application of zinc oxide in the form of nanorods. During hydrothermal synthesis, ZnO nanorods are formed in solution with precursors, and if a substrate with a seed layer is placed in the solution, nanorods will grow on the substrate. Therefore, to create biosensors, ZnO nanoparticles are applied directly from a suspension [24,45,46] or formed on a substrate with preformed seed layers [23,25,28]. The advantage of application from a suspension is the possibility of obtaining a given dispersion of particles by separating the particles

according to size by methods such as centrifugation or filtration. However, this approach seems unpromising for integration with microfluidic systems due to the poor adhesion of particles on substrates with electrodes. ZnO nanorods grown on a substrate seems to be more promising for this purpose. However, during the hydrothermal synthesis of nanorods on a substrate, they grow not only on the substrate, but also in the bulk of the solution, forming agglomerates which can be fixed on the sample surface. This worsens the reproducibility of the technology, since the process is random to a certain extent. In addition, the seed layer is applied by centrifugation [23,28], which, unlike the hydrothermal method, is not so convenient for scaling. Additionally, the use of methods for depositing a ZnO seed layer in a vacuum, such as the Magnetron sputtering technique [25], also somewhat reduces the advantages of the hydrothermal method, which does not require vacuum systems.

In this study, the hydrothermal synthesis of ZnO nanorods on the substrate surface was carried out with the suppression of nucleation in the bulk of the solution, making it more reproducible. Additionally, the ZnO seed layer was deposited by ultrasonic spray pyrolysis, which does not require a vacuum and is easily scaled up, similar to the hydrothermal method. We believe that cost effectiveness and scalability play an important role in terms of future prospects for creating commercial sensor platforms. Therefore, the purpose of this work was to study the possibility of using this technique for the synthesis of coatings from nanorods to develop an impedimetric biosensor on interdigitated electrodes.

2. Materials and Methods

2.1. *In Vitro* Study of Complex Formation between Protein A and Omalizumab

In this study, we decided to demonstrate the use of zinc oxide modified electrodes for the detection of omalizumab using surface-bound protein A.

Omalizumab (MW 149 kDa) is a humanized anti-IgE monoclonal IgG1 antibody used in the treatment of bronchial asthma [47]. It was produced in soluble form in the modified CHO cell line, then purified from the supernatant with Protein A affinity chromatography and with SEC to remove aggregates. The resulting purity of the omalizumab specimen used in this work was 96.8%, as determined with RP-HPLC.

Protein A (M_w 50 kDa in S-S dimer form) is a surface protein of *S. aureus*, able to bind IgG [48] and modified with His-tag and several amino acid substitutions. It was produced in a soluble form in the modified *E. coli* strain, then purified from the cell lysate with metal-chelate affinity chromatography on Ni-NTA resin and then with cation-exchange chromatography. The resulting purity of the protein A specimen used in this work was 97.6% as determined with RP-HPLC.

Both omalizumab and protein A specimens were kindly provided by S.V. Rodin.

To show their ability for complementary interaction, we conducted studies using Kapel-105M (Lumex Ltd., Saint Petersburg, Russia) capillary electrophoresis, with capillary inner diameter of 75 μm , a total length of 60 cm, an effective length of 50 cm, a temperature of +30 °C and a spectrophotometric detector with detection wavelength at 200 nm. To dilute the stock solutions, a 10 mM Tris-HCl buffer with a pH of 7.2 was used.

Electropherograms of stock solutions showed a single electrophoretic peak at 4.8 min for omalizumab (Figure 1) and 9.9 min for protein A (Figure 2).

The areas of both peaks were directly proportional to the concentration of the initial solutions.

2.2. Formation of an Electrode Coating from ZnO Nanorods

The biosensor was based on a ceramic substrate with NiCr/Ni/Au interdigitated electrodes (Sensor Platform, Tesla Blatna, a.s.). The width of the electrodes and the distance between the electrodes deposited on the substrate were 25 μm . Coating of the ZnO nanorods was performed by a two-stage procedure, consisting of ultrasonic spray pyrolysis of a zinc oxide seed layer and the low-temperature hydrothermal synthesis of nanorods with suppression of nucleation in the bulk solution. This technique allows a selective growth of nanorods to be realized only on the substrate surface. In the first stage, an aqueous

solution of 0.05 M zinc acetate (purity $\geq 99\%$, Vekton, Saint Petersburg, Russia) was used to deposit a ZnO seed film by ultrasonic spray pyrolysis for 5 min. The substrate heating temperature was maintained at $+380\text{ }^{\circ}\text{C}$. A control sample of the ZnO seed layer was formed on the polished side of the silicon substrate. The morphology of the seed layer was studied using atomic force microscopy (Atomic Force Microscope Probe nanolaboratory INTEGRA-TERMA, NT-MDT, Saint Petersburg, Russia) (Figure 3).

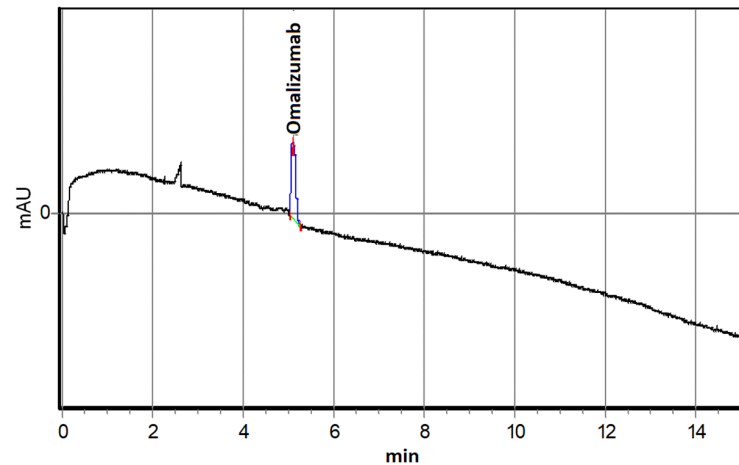


Figure 1. Electropherogram of an $0.6\text{ }\mu\text{M}$ Omalizumab solution.

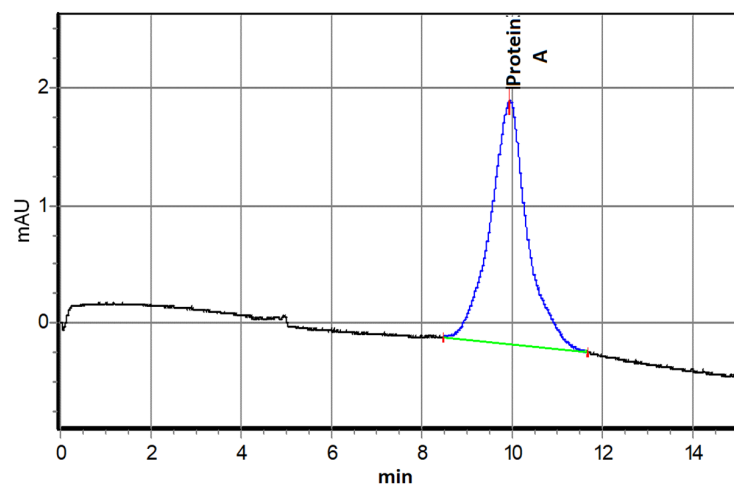


Figure 2. Capillary electrophoresis of $1.28\text{ }\mu\text{M}$ Protein A solution.

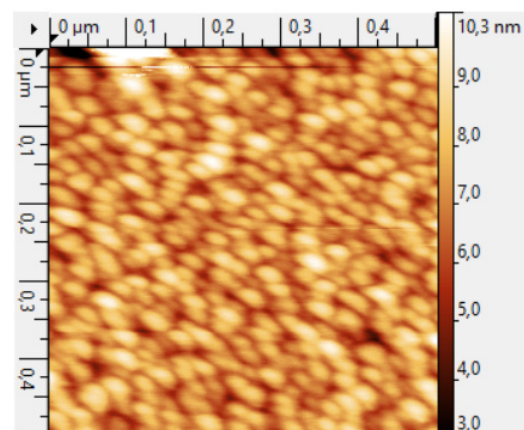


Figure 3. AFM image of the topography of a seed layer obtained by ultrasonic spray pyrolysis.

The roughness of the ZnO seed layer was ~ 10 nm, and the size of the crystallite width was 25–30 nm.

Low-temperature hydrothermal synthesis of ZnO nanorods from a seed layer was carried out using an aqueous solution of zinc nitrate (purity $\geq 98\%$, Vekton, Saint Petersburg Russia) and hexamethylenetetramine (purity $\geq 98\%$, Vekton, Saint Petersburg, Russia) with an equimolar concentration of 25 mM, to which ammonia water (purity $\geq 98\%$, Vekton, Saint Petersburg, Russia) and polyethyleneimine (branched, Mw ~ 800 , Sigma-Aldrich, St. Louis, MO, USA) were added to ensure ZnO nucleation in the bulk of the solution. The features of the synthesis of the ZnO nanorods have been described in more detail in [49]. After synthesis, the ZnO nanorods were annealed at a temperature of $+500$ °C for 5 min. The results of the scanning electron microscopy of a control sample on a silicon substrate are shown in Figure 4.

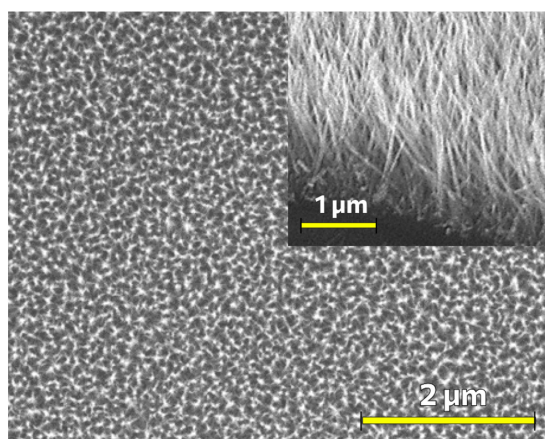


Figure 4. SEM micrograph of a coating of ZnO nanorods formed by a low-temperature hydrothermal method with suppression of nucleation in the bulk solution and the use of a seed layer formed by ultrasonic spray pyrolysis. The inset shows the cross-section of the sample.

As can be seen from the SEM micrograph (Figure 4), a uniform coating of ZnO nanorods of ~ 1 μm in length and with a diameter which does not exceed 50 nm was formed.

The surface of the ZnO nanorods was studied using X-ray photoelectron spectroscopy (XPS). The XPS study was carried out under ultrahigh vacuum conditions ($\sim 10^{-7}$ Pa) on an Escalab 250Xi complex photoelectron spectrometer (Thermo Fisher Scientific Inc., Waltham, MA, USA) at the excitation photon energy, $\text{AlK}\alpha$, of 1486 eV. The XPS spectra were processed using the CasaXPS Version 2.3.24 software.

2.3. Immobilization of Ligands on ZnO Nanorods

In the development and fabrication of a biosensor, an important step is the integration of a recognizing element into its structure that is capable of selectively capturing an analyte. The recognizing element must be immobilized on the surface of the electrode. For that, the electrodes surface must be functionalized with some reactive chemical groups, usually NH_2 - or SH - groups. The easiest way to functionalize the ZnO surface with NH_2 - groups is by treatment with aminosilanes, which can be achieved in many different ways with different silanes [50,51]. In this study, we used the method of (3-aminopropyl)trimethoxysilane (APTMS) treatment in water solutions. This method could be easily scaled-up for mass production of biosensor chips. The NH_2 - groups on surface could be then used for direct conjugation of various organic compounds, including antibodies, onto the substrate surface, or as an intermediate layer in multi-step conjugations.

In addition to chips with electrodes for the purpose of technological control, we also carried out silanization of glasses coated with a layer of zinc oxide nanorods using the same technology. ZnO was annealed to glass slides by heating at $+180$ °C for 10 min. Then, glasses were treated with 2% APTMS (Sigma-Aldrich 281778, $>97\%$, St. Louis, MO, USA) in isopropanol for 60 min, washed in isopropanol and dried in air at room temperature.

After silanization, electrodes and glass slides were functionalized with SH-groups by treatment with *m*-maleimidobenzoyl-*N*-hydroxysuccinimide ester (MBS) (Thermo Fisher Scientific 22311, Waltham, MA, USA) solution. The presence of SH- groups allows conjugation of ligands with more constant orientation as SH- groups are much less abundant in proteins than NH₂ groups. To prepare a solution of MBS, 5 mg of MBS was dissolved in 5 mL of dimethyl sulfoxide (DMSO), and then the mixture was dissolved in 20 mL of PBS (phosphate-buffered saline, 20 mM monosodium phosphate, 0.9% NaCl, pH 7.4, adjusted with NaOH). The substrate was treated with this solution for 70 min, washed with PBS and deionized water, and then dried in air at room temperature.

In the last step, protein A was conjugated to the chips and the glass slides treated with MBS through formation of S-S bonds. First, the SH- groups of protein A were reduced with dithiothreitol (DTT) (Sigma-Aldrich 111474, >99%, St. Louis, MO, USA). An amount of 5 mg of DTT was added to 100 µL of 10 mg/mL protein A solution in PBS, this solution was incubated at +40 °C for 1 h, then dissolved with PBS to 2 mg/mL and dialyzed against PBS in a dialysis bag with MWCO of 14 kDa (Sigma D-92777). Second, the reduced protein A was conjugated to chips and glasses treated with MBS in two steps: short-time conjugation with concentrated ligand for a short time and then long-time conjugation with diluted ligand for a long time. Initially, only some small areas on the chips which will be in further contact with analytes were treated with protein A solution after dialysis for 1 h. Next, 10 mL of PBS was added to the Petri dish with chips, and the samples were left on a shaker for 8 h. This was done to ensure the conjugation of protein A to the surface. After immobilization of protein A, the chips and slides were washed in buffer and water, dried in air and stored at +4 °C.

2.4. Impedance Spectroscopy

Impedance spectroscopy was implemented on the biochips for detection of the binding of the target substance, omalizumab, and was performed in the frequency range from 1 Hz to 500 kHz, with a voltage amplitude of 100 mV and without applying an additional DC bias (impedance meter Z500P, Elins, Chernogolovka, Russia). We decided to use this amplitude upon analysis of the experiments of scientific groups that detected cardiac troponin [24], as well as colleagues who worked on a similar device [52]. In the future, we plan to use the developed chip for multiparametric detection of protein biomarker arrays for diagnosis of chronic diseases. The measurement procedure (Figure 5) consisted of immersing the immobilized sensor in a 1.5 mL solution of omalizumab in PBS buffer (pH 7.4) with a concentration of 25 mM, where the sensor was kept for 5 min. Then, the sensor was further rinsed in 1.5 mL of deionized water to remove residual buffer solution and non-crosslinked omalizumab, and finally it was immersed in deionized water for impedance spectrum measurements. The sensor chip contacts were connected to the impedance meter via miniature clamps and shielded wires to minimize noise.

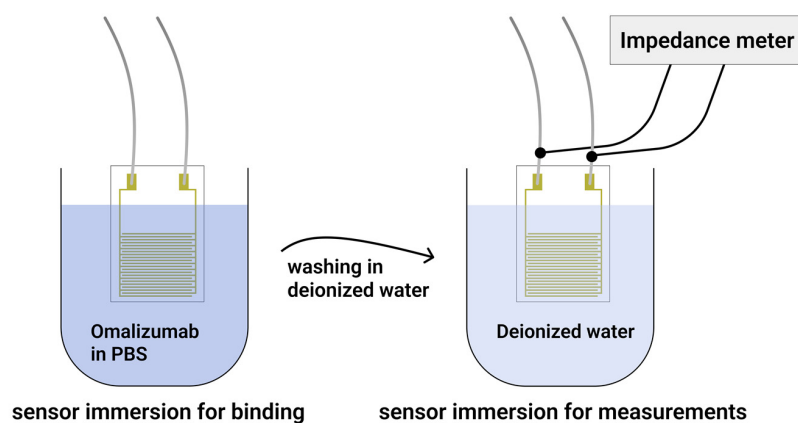


Figure 5. Schematic presentation of the measurement procedure stages.

3. Results and Discussion

The zinc oxide nanorods were obtained using hydrothermal synthesis on substrates with comb electrodes. The SEM micrograph of the nanorods on the surface of a ceramic substrate with an electrode is shown in Figure 6.

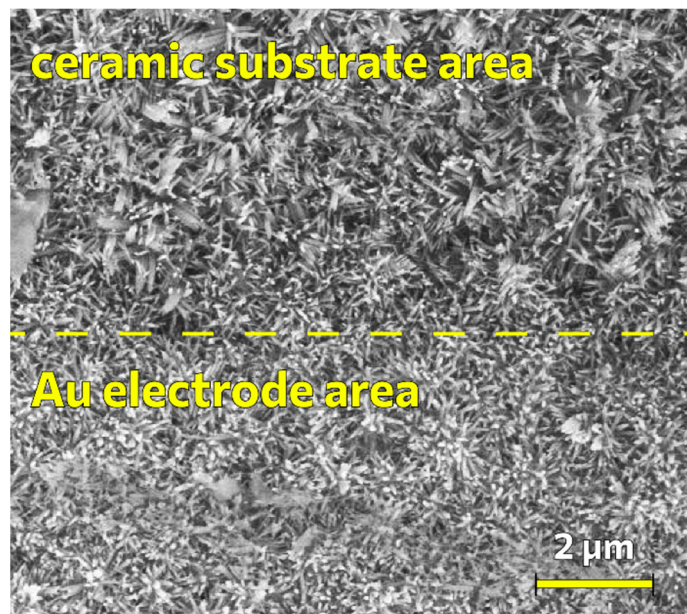


Figure 6. SEM micrograph of ZnO nanorods on the surface of a ceramic substrate with interdigitated electrodes.

It can be seen from Figure 6 that the morphology of the coating of ZnO nanorods on the surface of the ceramic substrate with interdigitated electrodes differs from the coating of nanorods on a silicon substrate, this is due to the morphology of the initial ceramic substrate, which consists of larger grains. The grain edges determine the general directivity for several nanorods at once.

It should be noted that the distance between the ZnO nanorods is large enough to effectively immobilize the nanorods, with protein A binding to omalizumab. The characteristic dimensions of such biological objects are in units of nanometers [53], while the distance between nanorods is tens of nanometers (Figures 4 and 6). Nevertheless, the nanorod diameter of ~50 nm is comparable with the total thickness of bounded biorecognition elements (>10 nm), since they are crosslinked from all sides of the nanorods. The resulting system can be considered as a composite material consisting of a zinc oxide phase and a phase of biorecognition elements, obviously differing in dielectric constant, ϵ , and polarization mechanisms. Moreover, since the crosslinking processes occur in the buffer solution, a double electric layer should form on the biosensor surface, which also affects the polarization processes. All these factors indicate that the geometric parameters of the nanostructured ZnO layer can have a significant effect on the features of the impedance spectra and the sensitivity of the sensor. The optimization of these parameters is a goal of our further research.

The results of X-ray photoelectron spectroscopy of the surface of ZnO nanorods are shown in Figure 7.

It can be seen from the survey XPS spectrum that, in addition to the core levels of zinc and oxygen, the core level of carbon C1s is observed, which is probably associated with the adsorption of carbon-containing compounds from the air. A detailed interpretation of the overview spectrum was made according to [54]. In addition to the main peaks of the Zn2p, O1s and C1s core levels, less intense peaks of photoelectrons of the Zn2s, Zn3p and Zn3d core levels of zinc, as well as Auger electrons O KLL and Zn LMM, were noted. The ratio of zinc atoms to oxygen was ~1.13. In this case, obviously, part of the oxygen is

contained in the surface-adsorbed groups, which makes the ratio of zinc to oxygen atoms even higher than 1.13. The detailed spectrum of the core oxygen level, O1s, shows the main oxygen peak in the zinc oxide crystal lattice (~ 530.9 eV) and a distinct second peak, which, according to the literature [55–58], is associated with oxygen in the adsorbed OH groups on the ZnO surface. Since carbon is observed on the surface of ZnO, part of the O1s spectrum must be due to oxygen in adsorbed compounds with carbon. The deconvolution of the O1s spectrum was carried out according to [55,56].

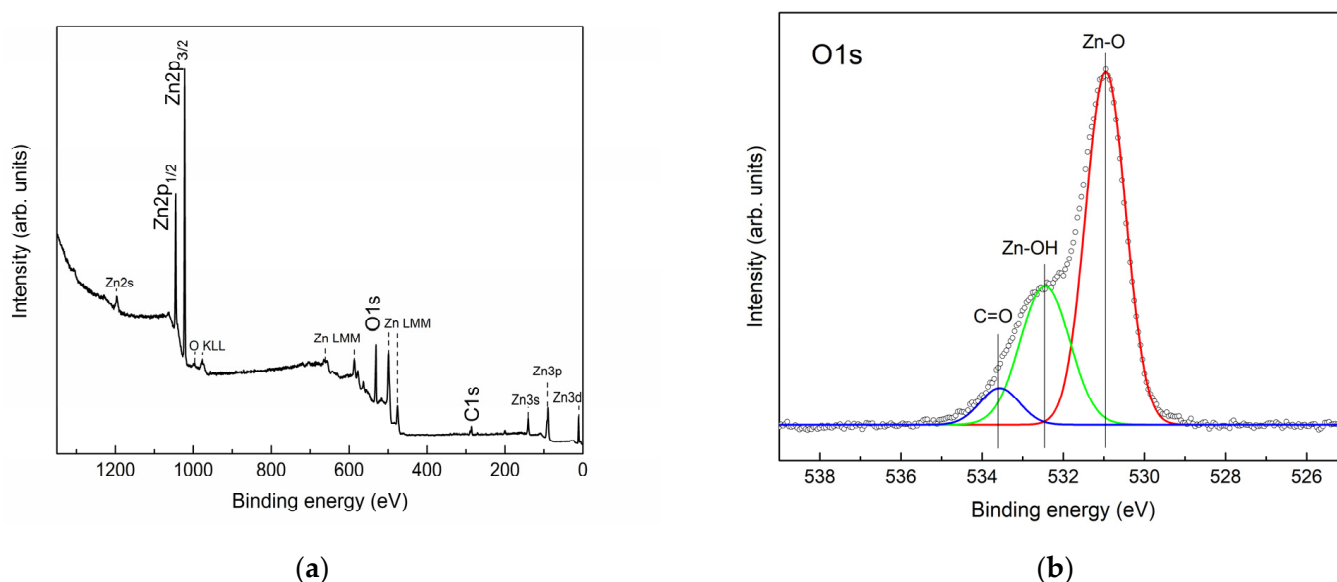


Figure 7. XPS spectra of the surface of ZnO nanorods: (a) survey spectrum of the ZnO surface; (b) spectrum of the core oxygen level, O1s.

We assume that the high concentration of oxygen vacancies and the predominance of zinc atoms in the ZnO surface layer promote the adsorption of -OH groups. In turn, the obtained ratio of oxygen atoms to zinc and oxygen can be associated not only with the processes of assembly of ZnO nanocrystals during hydrothermal synthesis, but to a greater extent to the process of annealing the samples at $500\text{ }^{\circ}\text{C}$ after synthesis. A high concentration of OH groups should contribute to the successful silanization process in our experiment.

As noted above, a high concentration of OH groups on the surface of ZnO is also accompanied by a high photocatalytic activity. This may be due to the formation of additional defective levels within the band gap, which are more energetically favorable for the formation of reactive oxygen species and OH radicals. As can be seen from the XPS data, the composition of the near-surface region of the synthesized ZnO is indeed significantly deviated from the stoichiometry. The ZnO nanorods used in this work can potentially have good photocatalytic activity. At the same time, standard glasses and some optically transparent polymeric materials that are used to create microfluidic systems will be transparent for the absorption edge of ZnO (~ 380 nm). Thus, photocatalytic decomposition on ZnO or similar metal oxide photocatalysts can be easily implemented for microfluidic systems.

Calibration relationships for omalizumab and protein A were obtained using the following solutions:

- Omalizumab: 0.2; 0.4; and 0.6 μM (Figure 8a);
- Protein A: 0.64; 1.28; 3.2; and 6.4 μM (Figure 8b).

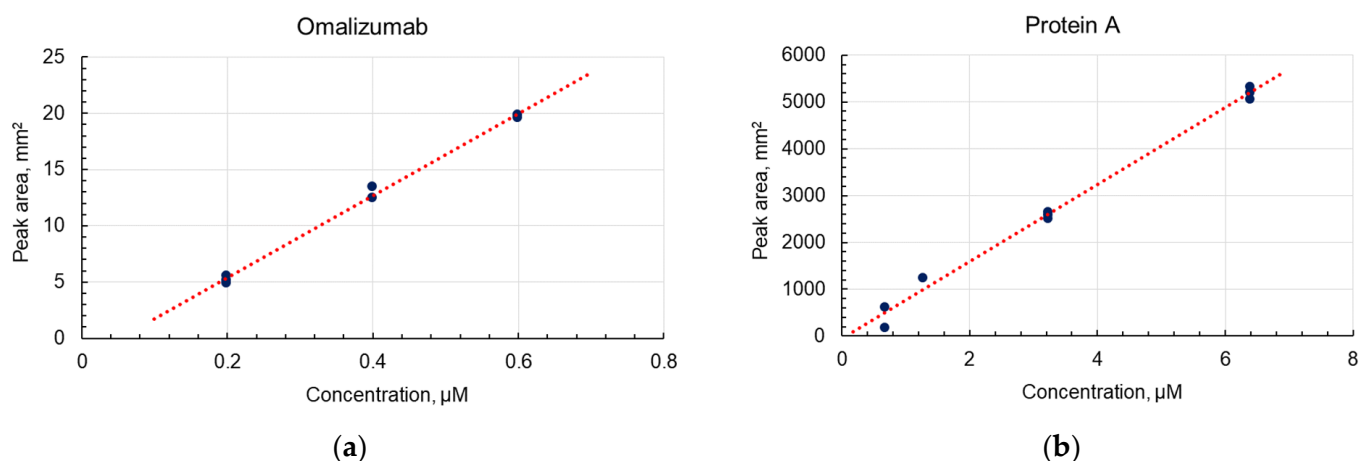


Figure 8. Concentration (μM) dependence of the electrophoretic peak area (mm^2): (a) omalizumab, $y = 36.434x - 1.9043$ ($R^2 = 0.9982$); (b) protein A, $y = 821.88x - 53.334$ ($R^2 = 0.9974$).

The complex formation of omalizumab and protein A in different molar ratios was studied with capillary electrophoresis. An example electropherogram of a mixture with a ratio of protein A/omalizumab of 1.06 is shown in Figure 9. All electropherograms of mixtures, regardless of the ratio of components, contained three zones, two of which were previously assigned to the initial components, while the third intermediate zone represents the resulting protein–antibody complex.

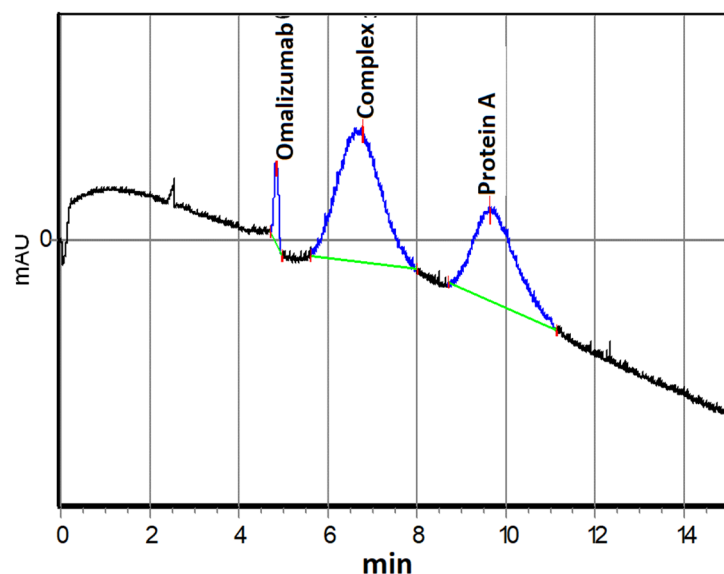


Figure 9. Electropherogram of a solution containing omalizumab ($0.6 \mu\text{M}$) and protein A ($0.64 \mu\text{M}$).

Using the capillary electrophoresis data, the average value of the effective dissociation constant of the 1:1 complex was determined, at $K_d = (5.1 \pm 2.1) \times 10^{-7}$ ($\text{p}K_d = 6.3$). Thus, the formation of a complex between omalizumab and protein A was demonstrated, which proved its further application for quality control of biosensor substrates and the sensitivity of the formed nanostructured biosensor element.

We tested the effectiveness of protein A immobilization on zinc oxide nanorods by detecting the binding of antibodies labeled with horseradish peroxidase. For this, glass substrates were washed in BBST pH 8.2 (20 mM borate buffer with 0.9% NaCl and 0.1% Tween-20) and treated with $0.2 \mu\text{g}/\text{mL}$ horseradish peroxidase antibody conjugate in BBST with $1 \text{ mg}/\text{mL}$ BSA (Sigma-Aldrich, >98%) for 1 h. Then, the substrates were washed in BBST and developed in 3,3',5,5'-tetramethylbenzidine (TMB). As a negative control, a glass

with nanorods of zinc oxide subjected only to silanization without treatment with MBS and protein A was used, and one glass with conjugated protein A was taken as the sample (Figure 10).

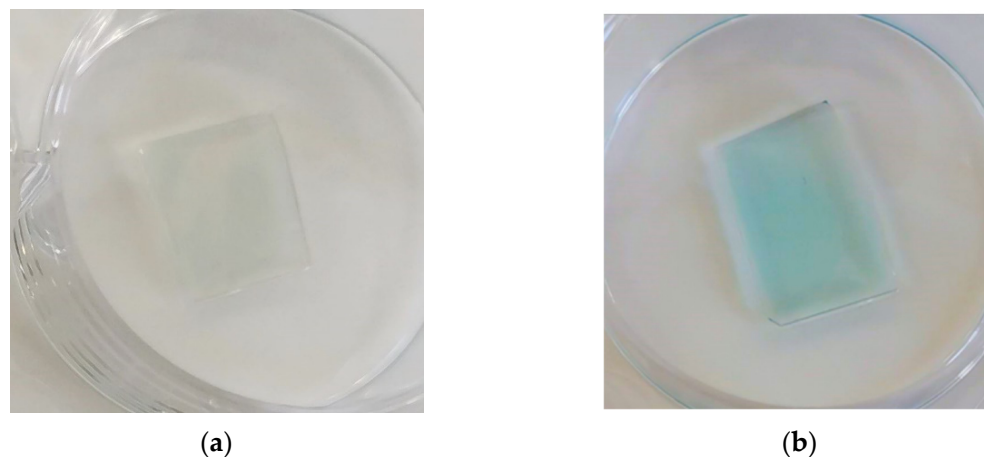


Figure 10. Detection of binding of horseradish peroxidase-conjugated antibodies to the surface of ZnO-coated glasses with bound protein A using TMB treatment: (a) glass with ZnO nanorods without MBS treatment, only silanized: negative control; (b) glass coated with zinc oxide nanorods silanized with MBS treatment.

A drop of TMB on the glass with protein A quickly began to turn blue and then yellow, which meant that TMB reacted with horseradish peroxidase. Horseradish peroxidase is associated with antibodies; therefore, this observation indicates that the antibodies have bound, meaning that protein A has been adsorbed onto the glass. Slight traces of staining are visible on the glass without treatment with protein A, which may indicate a small proportion of physical adsorption of the antibody. The obtained data indicate that protein A is adsorbed on the ZnO–silane–MBS structure in the operable state and orientation.

As a result of the study of the frequency range for measuring the impedance spectra of various concentrations of omalizumab, we determined the frequency range where the concentration dependence of the impedance is clearly visible (Figure 11).

The characteristic frequency range of the supplied alternating signal for the created biochip was approximately from 7 to 500 kHz in the total investigated range of 1 Hz–500 kHz. As can be seen from Figure 11, an increase in the concentration of the target antibody in the sample leads to a change in the impedance spectrum in the Nyquist coordinates of the biochip after it is immersed in the analyzed solution. With an increase in the concentration of the target antibody, omalizumab, a shift in the circular arc in the impedance spectrum is observed.

The impedance spectrum in the Nyquist coordinates for such systems of semiconductor nanorods has a characteristic semicircle shape and can be described by an equivalent RC scheme [52,59]. For composite organo–inorganic structures that are detected by electrochemical nanobiosensors, part of the impedance spectrum usually also has a distinct semicircle region [60–62]. However, as we assumed from the design of the experiment, despite the stage of washing and measurements in deionized water, the binding processes are also accompanied by the transfer of ions in the buffer solution (surrounding the proteins in the buffer). The impedance spectra indicate (Figure 11) an outline typical for an electrochemical system [60], where there is a circular arc region corresponding to the resistance of the electrolyte and ZnO nanorods and a characteristic “tail” of the corresponding electric double layer (EDL) diffusion region.

A decrease in the arc of the circle is characteristic of an increase in the concentration of electrolyte ions [52]. In our case, a decrease in the circular arc is observed with an increase in the concentration of the target protein, and, apparently, is accompanied by an increase in the concentration of bound buffer ions on the protein surface.

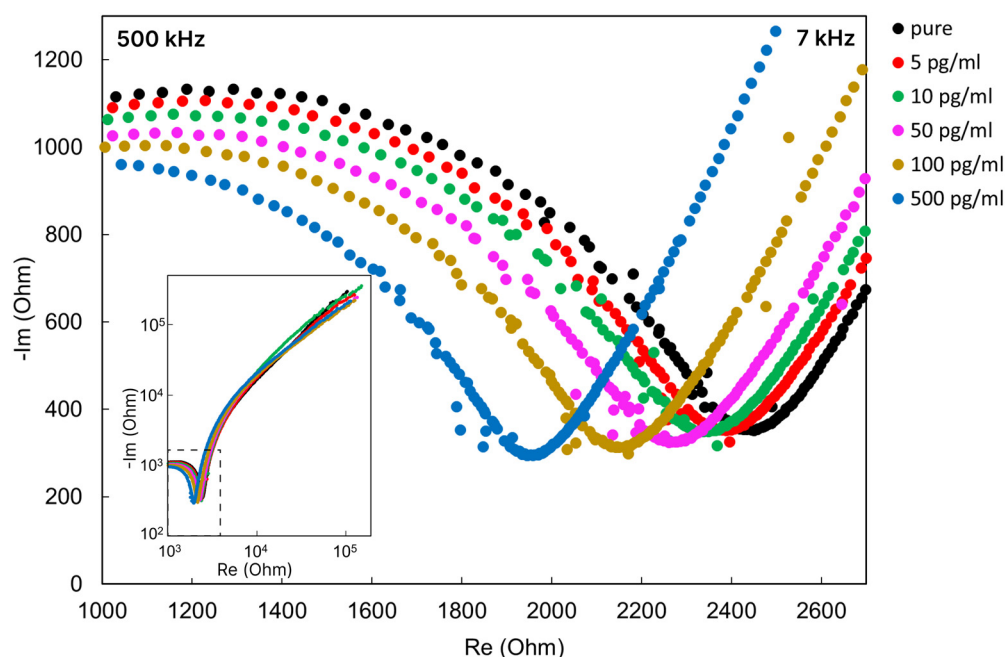


Figure 11. Nyquist plot for the biochip after immersion in omalizumab solutions of various concentrations.

Thus, the binding of omalizumab to protein A redistributes the charge in the near-electrode electric double layer (EDL). Tracking the EDL changes indicates biomolecular binding events [25]. The changes that occur with the formation of the near-electrode EDL at the boundary between the biosensor surface and the surrounding liquid can be successfully detected using electrical impedance spectroscopy. At the same time, the identification of the frequency range in which the maximum sensitivity and response is observed will make it possible to implement a simplified measurement scheme in the future, in the form of a portable device with a disposable line of sensitive electrodes and immobilized biorecognizing elements.

Based on the results of the impedance measurements, we determined the frequency range from 7 to 50 kHz, which allowed us to observe a linear change in the impedance in response to a change in the analyte concentration. Figure 12 shows the change in impedance of biochips with bound omalizumab versus the logarithm of concentration at a frequency of 12 kHz. The dependence for omalizumab impedance is linear for the studied concentration range and satisfies the linear equation: $y = 220.11x - 134.87$, with $R^2 = 0.9421$. The concentration limit of detection (LOD) for omalizumab was 5 pg/mL, which was calculated by a standard procedure using standard deviation and slope values.

In addition, for the same range of concentrations, we demonstrated a similar dependence for BSA solutions. The selection of BSA was motivated by the presence of this protein in blood samples in large concentrations; thus, it can be used to demonstrate the absence of non-specific binding. Compared to omalizumab solutions, the developed chips in BSA solutions showed almost the same impedance response over the studied concentration range, which indicates the absence of nonspecific binding between protein A and BSA. Therefore, we have demonstrated the operability of the developed biosensor structure and have determined the operating frequency range and good sensitivity. Further research will be carried out to create multisensor impedimetric microsystems for detecting various protein markers of diseases.

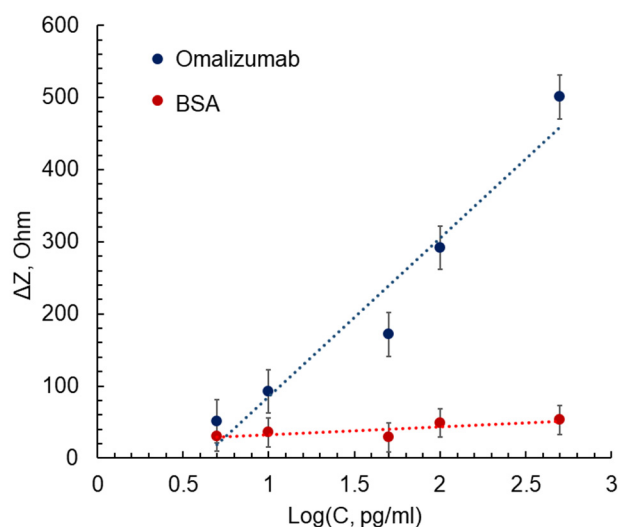


Figure 12. Dependences of the impedance change at a frequency of 10 kHz on the logarithm of the concentration of omalizumab (blue line, $y = 220.11x - 134.87$, $R^2 = 0.9421$) and BSA (red line, $y = 11.096x + 21.432$, $R^2 = 0.6464$).

4. Conclusions

Micro- and nano-technologies make it possible to implement the automatic control of the stages of analytical procedures using integrated functional modules in microsystems on the microscale. They enable flexible modeling of the topology and design of such systems for performing a specific analysis, and furthermore enable the creation of multichannel systems for parallel analysis of multiple samples.

Impedimetric sensors can be successfully combined with microfluidic systems [63,64], which promises the prospect of their use as sensor nodes in miniature analytical systems, such as in lab-on-a-chip systems. Unlike other electrochemical sensors, impedimetric sensors are less demanding in regard to the quality of the electrodes. They can be chemically stable in a variety of media and offer the ability to work in opaque samples, unlike most optical biosensors.

Modern biosensor systems should provide high sensitivity and selectivity, high detection rate, small sample volume, be small in size and have low cost. Ensuring this set of characteristics is possible due to the heterogeneous integration of functional modules into a single system, the architectonics of which determines a set of design and technological solutions implemented at the micro- and nano-levels, including those using biological media. The physical and technical principles of detection underlying the created biosensor system are often determined by the nature and properties of the analyzed biological component, in particular, protein structures identified as markers of diseases and physiological conditions. The development of registration methods without the use of specialized labels, which complicate and increase the cost of the design and technology of forming biosensor systems, is an object of interest for many researchers [65–67].

In this study, we demonstrated the operability of a label-free impedimetric biosensor for detecting antibodies using electrodes coated with zinc oxide nanorods. We performed a preliminary study of the binding of protein A and omalizumab using capillary electrophoresis. Zinc oxide nanorods were deposited by spray pyrolysis on comb electrodes, after which they were silanized and conjugated with protein A on the surface. Using impedance spectroscopy, it was possible to detect the binding of omalizumab at concentrations down to 5 pg/mL. We assume that the coating of electrodes with ZnO nanorods in the future will not only serve as a matrix for immobilization and increase the effective area of electrodes, but will also ensure the reusability of the biochip due to the cleaning of electrodes coated with ZnO by photocatalytic decomposition of the bound molecules.

Further development of this work should go towards the creation of highly sensitive multiparametric biosensor systems for the diagnosis of protein markers of diseases. To this end, we plan to create detection sites using peptide aptamers with spatial complementarity to target proteins. We have a set of tools and methods for an *in silico* search for such structures [68,69] and are currently testing a number of samples for protein markers of cardiovascular and inflammatory diseases. This is particularly important in relation to the prospect of using such biosensors in Point-of-Care systems.

Author Contributions: Conceptualization, N.S., A.R., A.K. (Alexey Kolobov), V.M. and T.Z.; methodology, N.S., A.R., A.K. (Alexey Kolobov), A.A., A.M., S.P., A.K. (Alexei Komolov), V.M. and T.Z.; software, S.P. and A.K. (Alexei Komolov); validation, N.S., A.R. and A.K. (Alexey Kolobov); formal analysis, A.A., A.M., S.P., A.K. (Alexei Komolov), V.M. and T.Z.; investigation, N.S., A.R., A.K. (Alexey Kolobov) and A.K. (Alexei Komolov); resources, N.S., A.R., A.K. (Alexei Komolov), A.K. (Alexey Kolobov), A.A., V.M. and T.Z.; data curation, A.A., A.M., A.K. (Alexei Komolov), S.P., V.M. and T.Z.; writing—original draft preparation, N.S. and A.R.; writing—review and editing, N.S., A.R. and T.Z.; visualization, N.S., A.R., A.K. (Alexey Kolobov), A.M. and A.K.; supervision, V.M. and T.Z.; project administration, N.S., A.R., V.M. and T.Z.; funding acquisition, N.S., A.R., A.K. (Alexey Kolobov), V.M., T.Z., A.K. (Alexei Komolov) and S.P. All authors have read and agreed to the published version of the manuscript.

Funding: N.S., A.K. (Alexey Kolobov) and T.Z. acknowledge support of the Russian Science Foundation, (Project No. 21-79-20219) for the material and technical support of research. A.K. (Alexei Komolov). and S.P. acknowledge the support of the Russian Science Foundation (Project No. 19-13-00021) for XPS measurements and spectral analysis. The measurements were partly taken using the equipment of the Research Park of St. Petersburg State University “Physical methods of surface investigation (Project No. 93021679)”.

Institutional Review Board Statement: Not applicable.

Informed Consent Statement: Not applicable.

Data Availability Statement: Not applicable.

Acknowledgments: The authors acknowledge with thanks Y.A. Skorik (Almazov National Medical Research Centre, Akkuratova 2, 197341 St. Petersburg, Russia) for their help with the electrophoretic study of omalizumab and protein A interactions.

Conflicts of Interest: The authors declare no conflict of interest.

References

1. Samuel, V.; Rao, K.J. A Review on Label Free Biosensors. *Biosens. Bioelectron. X* **2022**, *11*, 100216. [[CrossRef](#)]
2. Sohrabi, H.; Bolandi, N.; Hemmati, A.; Eyvazi, S.; Ghasemzadeh, S.; Baradaran, B.; Oroojalian, F.; Reza Majidi, M.; de la Guardia, M.; Mokhtarzadeh, A. State-of-the-Art Cancer Biomarker Detection by Portable (Bio) Sensing Technology: A Critical Review. *Microchem. J.* **2022**, *177*, 107248. [[CrossRef](#)]
3. Alhalaili, B.; Popescu, I.N.; Rusanescu, C.O.; Vidu, R. Microfluidic Devices and Microfluidics-Integrated Electrochemical and Optical (Bio)Sensors for Pollution Analysis: A Review. *Sustainability* **2022**, *14*, 12844. [[CrossRef](#)]
4. Dkhar, D.S.; Kumari, R.; Malode, S.J.; Shetti, N.P.; Chandra, P. Integrated Lab-On-a-Chip Devices: Fabrication Methodologies, Transduction System for Sensing Purposes. *J. Pharm. Biomed. Anal.* **2023**, *223*, 115120. [[CrossRef](#)] [[PubMed](#)]
5. Jaisankar, A.; Krishnan, S.; Rangasamy, L. Recent Developments of Aptamer-Based Lateral Flow Assays for Point-of-Care (POC) Diagnostics. *Anal. Biochem.* **2022**, *655*, 114874. [[CrossRef](#)] [[PubMed](#)]
6. Sitkov, N.; Zimina, T.; Kolobov, A.; Sevostyanov, E.; Trushlyakova, V.; Luchinin, V.; Krasichkov, A.; Markelov, O.; Galagudza, M.; Kaplun, D. Study of the Fabrication Technology of Hybrid Microfluidic Biochips for Label-Free Detection of Proteins. *Micromachines* **2022**, *13*, 20. [[CrossRef](#)]
7. Calidonio, J.M.; Hamad-Schifferli, K. Biophysical and Biochemical Insights in the Design of Immunoassays. *Biochim. Biophys. Acta (BBA)—Gen. Subj.* **2023**, *1867*, 130266. [[CrossRef](#)]
8. Warren, A.D.; Kwong, G.A.; Wood, D.K.; Lin, K.Y.; Bhatia, S.N. Point-of-Care Diagnostics for Noncommunicable Diseases Using Synthetic Urinary Biomarkers and Paper Microfluidics. *Proc. Natl. Acad. Sci. USA* **2014**, *111*, 3671–3676. [[CrossRef](#)]
9. Serin, M.; Kara, P. Biosensing Strategies (Approaches) for Diagnosis and Monitoring of Multiple Sclerosis. *Talanta* **2023**, *252*, 123794. [[CrossRef](#)]

10. Avgerinos, K.I.; Ferrucci, L.; Kapogiannis, D. Effects of Monoclonal Antibodies against Amyloid- β on Clinical and Biomarker Outcomes and Adverse Event Risks: A Systematic Review and Meta-Analysis of Phase III RCTs in Alzheimer's Disease. *Ageing Res. Rev.* **2021**, *68*, 101339. [[CrossRef](#)]
11. Banerjee, S.; Drapkin, R.; Richardson, D.L.; Birrer, M. Targeting NaPi2b in Ovarian Cancer. *Cancer Treat. Rev.* **2023**, *112*, 102489. [[CrossRef](#)] [[PubMed](#)]
12. Roberts, A.; Gandhi, S. A Brief Review on Novel Biomarkers Identified and Advanced Biosensing Technologies Developed for Rapid Diagnosis of Japanese Encephalitis Virus. *Proc. Indian Natl. Sci. Acad.* **2022**, *88*, 617–662. [[CrossRef](#)]
13. Chen, C.; Lehr, J. Label-free Selective Detection of Protein Markers in the Picomolar Range via a Convenient Voltammetric Sensing Strategy. *Electroanalysis* **2021**, *33*, 563–567. [[CrossRef](#)]
14. Qureshi, A.; Gurbuz, Y.; Niazi, J.H. Biosensors for Cardiac Biomarkers Detection: A Review. *Sens. Actuators B Chem.* **2012**, *171*–172, 62–76. [[CrossRef](#)]
15. Kimura, H.; Asano, R. Strategies to Simplify Operation Procedures for Applying Labeled Antibody-Based Immunosensors to Point-of-Care Testing. *Anal. Biochem.* **2022**, *654*, 114806. [[CrossRef](#)]
16. Menon, S.; Mathew, M.R.; Sam, S.; Keerthi, K.; Kumar, K.G. Recent Advances and Challenges in Electrochemical Biosensors for Emerging and Re-Emerging Infectious Diseases. *J. Electroanal. Chem.* **2020**, *878*, 114596. [[CrossRef](#)]
17. Alshanski, I.; Sukhran, Y.; Mervinetsky, E.; Unverzagt, C.; Yitzchaik, S.; Hurevich, M. Electrochemical Biosensing Platform Based on Complex Biantennary N-Glycan for Detecting Enzymatic Sialylation Processes. *Biosens. Bioelectron.* **2021**, *172*, 112762. [[CrossRef](#)]
18. Zeng, J.; Duarte, P.A.; Ma, Y.; Savchenko, O.; Shoute, L.; Khaniani, Y.; Babiuk, S.; Zhuo, R.; Abdelrasoul, G.N.; Charlton, C.; et al. An Impedimetric Biosensor for COVID-19 Serology Test and Modification of Sensor Performance via Dielectrophoresis Force. *Biosens. Bioelectron.* **2022**, *213*, 114476. [[CrossRef](#)]
19. Soma, F.N.; Khoris, I.M.; Chowdhury, A.D.; Boonyakida, J.; Park, E.Y. Impedimetric Biosensor of Norovirus with Low Variance Using Simple Bioconjugation on Conductive Polymer-Au Nanocomposite. *SSRN Electron. J.* **2022**. [[CrossRef](#)]
20. Solaimuthu, A.; Vijayan, A.N.; Murali, P.; Korrapati, P.S. Nano-Biosensors and Their Relevance in Tissue Engineering. *Curr. Opin. Biomed. Eng.* **2020**, *13*, 84–93. [[CrossRef](#)]
21. Zimina, T.M.; Sitkov, N.O.; Gareev, K.G.; Fedorov, V.; Grouzdev, D.; Koziava, V.; Gao, H.; Combs, S.E.; Shevtsov, M. Biosensors and Drug Delivery in Oncotheranostics Using Inorganic Synthetic and Biogenic Magnetic Nanoparticles. *Biosensors* **2022**, *12*, 789. [[CrossRef](#)] [[PubMed](#)]
22. Eivazzadeh-Keihan, R.; Bahojb Noruzi, E.; Chidar, E.; Jafari, M.; Davoodi, F.; Kashtiaray, A.; Ghafori Gorab, M.; Masoud Hashemi, S.; Javanshir, S.; Ahangari Cohan, R.; et al. Applications of Carbon-Based Conductive Nanomaterials in Biosensors. *Chem. Eng. J.* **2022**, *442*, 136183. [[CrossRef](#)]
23. Sanguino, P.; Monteiro, T.; Bhattacharyya, S.R.; Dias, C.J.; Igreja, R.; Franco, R. ZnO Nanorods as Immobilization Layers for Interdigitated Capacitive Immunosensors. *Sens. Actuators B Chem.* **2014**, *204*, 211–217. [[CrossRef](#)]
24. Yang, W.-C.; Liao, S.-Y.; Phan, T.L.; Van Hieu, N.; Chu, P.-Y.; Yi, C.-C.; Wu, H.-J.; Chang, K.-M.; Ching, C.T.-S. An Immunosensor for the Detection of ULBP2 Biomarker. *Micromachines* **2020**, *11*, 568. [[CrossRef](#)]
25. Shanmugam, N.R.; Muthukumar, S.; Selvam, A.P.; Prasad, S. Electrochemical Nanostructured ZnO Biosensor for Ultrasensitive Detection of Cardiac Troponin-T. *Nanomedicine* **2016**, *11*, 1345–1358. [[CrossRef](#)]
26. Cao, L.; Kiely, J.; Piano, M.; Luxton, R. Facile and Inexpensive Fabrication of Zinc Oxide Based Bio-Surfaces for C-Reactive Protein Detection. *Sci. Rep.* **2018**, *8*, 12687. [[CrossRef](#)]
27. Dong, S.; Zhang, D.; Cui, H.; Huang, T. ZnO/Porous Carbon Composite from a Mixed-Ligand MOF for Ultrasensitive Electrochemical Immunosensing of C-Reactive Protein. *Sens. Actuators B Chem.* **2019**, *284*, 354–361. [[CrossRef](#)]
28. Gasparotto, G.; Costa, J.P.C.; Costa, P.I.; Zaghete, M.A.; Mazon, T. Electrochemical Immunosensor Based on ZnO Nanorods-Au Nanoparticles Nanohybrids for Ovarian Cancer Antigen CA-125 Detection. *Mater. Sci. Eng. C* **2017**, *76*, 1240–1247. [[CrossRef](#)]
29. Jaiswal, N.; Pandey, C.M.; Solanki, S.; Tiwari, I.; Malhotra, B.D. An Impedimetric Biosensor Based on Electrophoretically Assembled ZnO Nanorods and Carboxylated Graphene Nanoflakes on an Indium Tin Oxide Electrode for Detection of the DNA of Escherichia Coli O157:H7. *Microchim. Acta* **2019**, *187*, 1. [[CrossRef](#)]
30. Khosravi-Nejad, F.; Teimouri, M.; Jafari Marandi, S.; Shariati, M. The Highly Sensitive Impedimetric Biosensor in Label Free Approach for Hepatitis B Virus DNA Detection Based on Tellurium Doped ZnO Nanowires. *Appl. Phys. A* **2019**, *125*, 616. [[CrossRef](#)]
31. Özgür, Ü.; Alivov, Y.I.; Liu, C.; Teke, A.; Reshchikov, M.A.; Doğan, S.; Avrutin, V.; Cho, S.-J.; Morkoç, H. A Comprehensive Review of ZnO Materials and Devices. *J. Appl. Phys.* **2005**, *98*, 041301. [[CrossRef](#)]
32. Bobkov, A.; Varezchnikov, A.; Plugin, I.; Fedorov, F.S.; Trouillet, V.; Geckle, U.; Sommer, M.; Goffman, V.; Moshnikov, V.; Sysoev, V. The Multisensor Array Based on Grown-On-Chip Zinc Oxide Nanorod Network for Selective Discrimination of Alcohol Vapors at Sub-Ppm Range. *Sensors* **2019**, *19*, 4265. [[CrossRef](#)] [[PubMed](#)]
33. Ryabko, A.A.; Nalimova, S.S.; Maximov, A.I.; Moshnikov, V.A. Investigation of the Gas Sensitivity of Nanostructured Layers Based on Zinc Oxide Nanorods under Ultraviolet Irradiation. In Proceedings of the 2021 IEEE Conference of Russian Young Researchers in Electrical and Electronic Engineering (ElConRus), Moscow, Russia, 26–29 January 2021. [[CrossRef](#)]
34. De Almeida, J.C.; Corrêa, M.T.; Koga, R.H.; Del Duque, D.M.S.; Lopes, O.F.; da Silva, G.T.S.T.; Ribeiro, C.; de Mendonça, V.R. Crystallization Time in ZnO: The Role of Surface OH Groups in Its Photoactivity. *New J. Chem.* **2020**, *44*, 18216–18224. [[CrossRef](#)]

35. Al-Sabahi, J.; Bora, T.; Al-Abri, M.; Dutta, J. Controlled Defects of Zinc Oxide Nanorods for Efficient Visible Light Photocatalytic Degradation of Phenol. *Materials* **2016**, *9*, 238. [[CrossRef](#)]
36. Redkin, A.N.; Ryzhova, M.V.; Yakimov, E.E.; Gruzintsev, A.N. Aligned Arrays of Zinc Oxide Nanorods on Silicon Substrates. *Semiconductors* **2013**, *47*, 252–258. [[CrossRef](#)]
37. Kawakami, M.; Hartanto, A.B.; Nakata, Y.; Okada, T. Synthesis of ZnO Nanorods by Nanoparticle Assisted Pulsed-Laser Deposition. *Jpn. J. Appl. Phys.* **2003**, *42 Pt 2*, L33–L35. [[CrossRef](#)]
38. Wu, J.-J.; Liu, S.-C. Low-Temperature Growth of Well-Aligned ZnO Nanorods by Chemical Vapor Deposition. *Adv. Mater.* **2002**, *14*, 215–218. [[CrossRef](#)]
39. Kim, S.-W.; Fujita, S.; Fujita, S. ZnO Nanowires with High Aspect Ratios Grown by Metalorganic Chemical Vapor Deposition Using Gold Nanoparticles. *Appl. Phys. Lett.* **2005**, *86*, 153119. [[CrossRef](#)]
40. Tien, L.C.; Norton, D.P.; Pearton, S.J.; Wang, H.-T.; Ren, F. Nucleation Control for ZnO Nanorods Grown by Catalyst-Driven Molecular Beam Epitaxy. *Appl. Surf. Sci.* **2007**, *253*, 4620–4625. [[CrossRef](#)]
41. Li, G.-R.; Dawa, C.-R.; Bu, Q.; Zhen, F.; Lu, X.-H.; Ke, Z.-H.; Hong, H.-E.; Yao, C.-Z.; Liu, P.; Tong, Y.-X. Electrochemical Synthesis of Orientation-Ordered ZnO Nanorod Bundles. *Electrochem. Commun.* **2007**, *9*, 863–868. [[CrossRef](#)]
42. Di Mauro, A.; Zimbone, M.; Fragalà, M.E.; Impellizzeri, G. Synthesis of ZnO Nanofibers by the Electrospinning Process. *Mater. Sci. Semicond. Processing* **2016**, *42*, 98–101. [[CrossRef](#)]
43. Joo, J.; Chow, B.Y.; Prakash, M.; Boyden, E.S.; Jacobson, J.M. Face-Selective Electrostatic Control of Hydrothermal Zinc Oxide Nanowire Synthesis. *Nat. Mater.* **2011**, *10*, 596–601. [[CrossRef](#)]
44. Xu, S.; Wang, Z.L. One-Dimensional ZnO Nanostructures: Solution Growth and Functional Properties. *Nano Res.* **2011**, *4*, 1013–1098. [[CrossRef](#)]
45. Zhang, Y.; Zhang, Z.; Rong, S.; Yu, H.; Gao, H.; Sha, Q.; Ding, P.; Pan, H.; Chang, D. A Sandwich-Type ECL Immunosensor Based on Signal Amplification Using a ZnO Nanorods-L-Cysteine-Luminol Nano-composite for Ultrasensitive Detection of Prostate Specific Antigen. *Anal. Chim. Acta* **2020**, *1109*, 98–106. [[CrossRef](#)] [[PubMed](#)]
46. Eveness, J.; Cao, L.; Kiely, J.; Luxton, R. Equivalent Circuit Model of a Non-Faradaic Impedimetric ZnO Nano-Crystal Biosensor. *J. Electroanal. Chem.* **2022**, *906*, 116003. [[CrossRef](#)]
47. McCarthy, M.W.; Aguilar-Zapata, D.; Petraitis, V.; Walsh, T.J. Diagnosis, Classification, and Therapeutic Interventions for Sinopulmonary Aspergillosis. *Expert Rev. Respir. Med.* **2017**, *11*, 229–238. [[CrossRef](#)] [[PubMed](#)]
48. Hober, S.; Nord, K.; Linhult, M. Protein A Chromatography for Antibody Purification. *J. Chromatogr. B* **2007**, *848*, 40–47. [[CrossRef](#)]
49. Ryabko, A.A.; Maximov, A.I.; Verbitskii, V.N.; Levitskii, V.S.; Moshnikov, V.A.; Terukov, E.I. Two-Stage Synthesis of Structured Microsystems Based on Zinc-Oxide Nanorods by Ultrasonic Spray Pyrolysis and the Low-Temperature Hydrothermal Method. *Semiconductors* **2020**, *54*, 1496–1502. [[CrossRef](#)]
50. Khan, S.; Rasheed, M.A.; Rafiq, M.A.; Shah, G.B.; Rehman, W.; Jamil, A.; Khan, Y. Silanization of ZnO Nanofibers by Tetraethoxysilane. *J. Appl. Polym. Sci.* **2017**, *134*, 45378. [[CrossRef](#)]
51. García Núñez, C.; Sachsenhauser, M.; Blashcke, B.; García Marín, A.; Garrido, J.A.; Pau, J.L. Effects of Hydroxylation and Silanization on the Surface Properties of ZnO Nanowires. *ACS Appl. Mater. Interfaces* **2015**, *7*, 5331–5337. [[CrossRef](#)]
52. Kondratev, V.M.; Morozov, I.A.; Vyacheslavova, E.A.; Kirilenko, D.A.; Kuznetsov, A.; Kadinskaya, S.A.; Nalimova, S.S.; Moshnikov, V.A.; Gudovskikh, A.S.; Bolshakov, A.D. Silicon Nanowire-Based Room-Temperature Multi-Environment Ammonia Detection. *ACS Appl. Nano Mater.* **2022**, *5*, 9940–9949. [[CrossRef](#)]
53. Erickson, H.P. Size and Shape of Protein Molecules at the Nanometer Level Determined by Sedimentation, Gel Filtration, and Electron Microscopy. *Biol. Proced. Online* **2009**, *11*, 32–51. [[CrossRef](#)] [[PubMed](#)]
54. Iaiche, S.; Djelloul, A. ZnO/ZnAl₂O₄ Nanocomposite Films Studied by X-ray Diffraction, FTIR, and X-Ray Photoelectron Spectroscopy. *J. Spectrosc.* **2015**, *2015*, 836859. [[CrossRef](#)]
55. Kwoka, M.; Kulis-Kapuscinska, A.; Zappa, D.; Comini, E.; Szuber, J. Novel Insight on the Local Surface Properties of ZnO Nanowires. *Nanotechnology* **2020**, *31*, 465705. [[CrossRef](#)] [[PubMed](#)]
56. Al-Gaashani, R.; Radiman, S.; Daud, A.R.; Tabet, N.; Al-Douri, Y. XPS and Optical Studies of Different Morphologies of ZnO Nanostructures Prepared by Microwave Methods. *Ceram. Int.* **2013**, *39*, 2283–2292. [[CrossRef](#)]
57. Grånäs, E.; Busch, M.; Arndt, B.; Creutzburg, M.; Semione, G.D.L.; Gustafson, J.; Schaefer, A.; Vonk, V.; Grönbeck, H.; Stierle, A. Role of Hydroxylation for the Atomic Structure of a Non-Polar Vicinal Zinc Oxide. *Commun. Chem.* **2021**, *4*, 7. [[CrossRef](#)]
58. Heinhold, R.; Allen, M.W. Polarity-Dependent Photoemission of in Situ Cleaved Zinc Oxide Single Crystals. *J. Mater. Res.* **2012**, *27*, 2214–2219. [[CrossRef](#)]
59. Schipani, F.; Miller, D.R.; Ponce, M.A.; Aldao, C.M.; Akbar, S.A.; Morris, P.A.; Xu, J.C. Conduction Mechanisms in SnO₂ Single-Nanowire Gas Sensors: An Impedance Spectroscopy Study. *Sens. Actuators B Chem.* **2017**, *241*, 99–108. [[CrossRef](#)]
60. Mei, B.-A.; Munteshari, O.; Lau, J.; Dunn, B.; Pilon, L. Physical Interpretations of Nyquist Plots for EDLC Electrodes and Devices. *J. Phys. Chem. C* **2017**, *122*, 194–206. [[CrossRef](#)]
61. Tran, D.T.; Vermeeren, V.; Grieten, L.; Wenmackers, S.; Wagner, P.; Pollet, J.; Janssen, K.P.F.; Michiels, L.; Lammertyn, J. Nanocrystalline Diamond Impedimetric Aptasensor for the Label-Free Detection of Human IgE. *Biosens. Bioelectron.* **2011**, *26*, 2987–2993. [[CrossRef](#)]
62. Narang, J.; Malhotra, N.; Singh, G.; Pundir, C.S. Electrochemical Impedimetric Detection of Anti-HIV Drug Taking Gold Nano-rods as a Sensing Interface. *Biosens. Bioelectron.* **2015**, *66*, 332–337. [[CrossRef](#)]

63. Schmidt-Speicher, L.M.; Länge, K. Microfluidic Integration for Electrochemical Biosensor Applications. *Curr. Opin. Electrochem.* **2021**, *29*, 100755. [[CrossRef](#)]
64. Nah, J.S.; Barman, S.C.; Zahed, M.A.; Sharifuzzaman, M.; Yoon, H.; Park, C.; Yoon, S.; Zhang, S.; Park, J.Y. A Wearable Microfluidics-Integrated Impedimetric Immunosensor Based on Ti3C2T MXene Incorporated Laser-Burned Graphene for Noninvasive Sweat Cortisol Detection. *Sens. Actuators B Chem.* **2021**, *329*, 129206. [[CrossRef](#)]
65. Upasham, S.; Banga, I.K.; Jagannath, B.; Paul, A.; Lin, K.-C.; Muthukumar, S.; Prasad, S. Electrochemical Impedimetric Biosensors, Featuring the Use of Room Temperature Ionic Liquids (RTILs): Special Focus on Non-Faradaic Sensing. *Biosens. Bioelectron.* **2021**, *177*, 112940. [[CrossRef](#)] [[PubMed](#)]
66. Antiochia, R. Electrochemical Biosensors for SARS-CoV-2 Detection: Voltametric or Impedimetric Transduction? *Bioelectrochemistry* **2022**, *147*, 108190. [[CrossRef](#)]
67. Magar, H.S.; Hassan, R.Y.A.; Mulchandani, A. Electrochemical Impedance Spectroscopy (EIS): Principles, Construction, and Biosensing Applications. *Sensors* **2021**, *21*, 6578. [[CrossRef](#)]
68. Sitkov, N.; Zimina, T.; Kolobov, A.; Karasev, V.; Romanov, A.; Luchinin, V.; Kaplun, D. Toward Development of a Label-Free Detection Technique for Microfluidic Fluorometric Peptide-Based Biosensor Systems. *Micromachines* **2021**, *12*, 691. [[CrossRef](#)]
69. Karasev, V. Data on the Application of the Molecular Vector Machine Model: A Database of Protein Pentapeptides and Computer Software for Predicting and Designing Secondary Protein Structures. *Data Brief* **2020**, *28*, 104815. [[CrossRef](#)]

Disclaimer/Publisher's Note: The statements, opinions and data contained in all publications are solely those of the individual author(s) and contributor(s) and not of MDPI and/or the editor(s). MDPI and/or the editor(s) disclaim responsibility for any injury to people or property resulting from any ideas, methods, instructions or products referred to in the content.